Low-temperature growth of dense and hard Ti0.41Al0.51Ta0.08N films via hybrid HIPIMS/DC magnetron co-sputtering with synchronized metal-ion irradiation

Hanna Fager, Olof Tengstrand, Jun Lu, S. Bolz, B. Mesic, W. Koelker, Ch. Schiffers, O. Lemmer, Joseph E Greene, Lars Hultman, Ivan Petrov and Grzegorz Greczynski

The self-archived version of this journal article is available at Linköping University Electronic Press:
http://urn.kb.se/resolve?urn=urn:nbn:se:liu:diva-137835

N.B.: When citing this work, cite the original publication.
Fager, H., Tengstrand, O., Lu, J., Bolz, S., Mesic, B., Koelker, W., Schiffers, C., Lemmer, O., Greene, J. E, Hultman, L., Petrov, I., Greczynski, G., (2017), Low-temperature growth of dense and hard Ti0.41Al0.51Ta0.08N films via hybrid HIPIMS/DC magnetron co-sputtering with synchronized metal-ion irradiation, *Journal of Applied Physics*, 121(17). https://dx.doi.org/10.1063/1.4977818

Original publication available at:
https://dx.doi.org/10.1063/1.4977818
Copyright: AIP Publishing
http://www.aip.org/

LINKÖPINGS UNIVERSITET

Low-temperature growth of dense and hard $Ti_{0.41}Al_{0.51}Ta_{0.08}N$ films via hybrid HIPIMS/DC magnetron co-sputtering with synchronized metal-ion irradiation

H.Fager,[1] O. Tengstrand,[1 a)] J. Lu,[1] S. Bolz,[2] B. Mesic,[2] W. Kölker,[2]
Ch. Schiffers,[2] O.Lemmer,[2] J. E. Greene,[1,3] L. Hultman[1], I. Petrov,[1,3]
G. Greczynski,[1]

[1] *Thin Film Physics Division, Department of Physics, Chemistry, and Biology (IFM), Linköping University, SE-581 83 Linköping, Sweden*
[2] *CemeCon AG, Adenauerstr. 20 A4, D-52146 Würselen, Germany*
[3] *Frederick Seitz Materials Research Laboratory and Materials Science Department, University of Illinois, 104 South Goodwin, Urbana, Illinois 61801, USA*

Hard $Ti_{1-x}Al_xN$ thin films are of importance for metal-cutting applications. The hardness, thermal stability, and oxidation resistance of these coatings can be further enhanced by alloying with TaN. We use a hybrid high-power pulsed and dc magnetron co-sputtering (HIPIMS/DCMS) technique to grow dense and hard $Ti_{0.41}Al_{0.51}Ta_{0.08}N$ alloys without external heating (T_s < 150 ºC). Separate Ti and Al targets operating in DCMS mode maintain a deposition rate of ~50 nm/min, while irradiation of the growing film by heavy Ta^+/Ta^{2+} ions from the HIPIMS-powered Ta target, using dc bias synchronized to the metal-ion-rich part of each HIPIMS pulse, provides effective near-surface atomic mixing resulting in densification. The substrate is maintained at floating potential between the short bias pulses to minimize Ar^+ bombardment which typically leads to high compressive stress. Transmission and scanning electron microscopy analyses reveal dramatic differences in the microstructure of the co-sputtered HIPIMS/DCMS films (Ta-HIPIMS) compared to films with the same composition grown at floating potential with all targets in DCMS mode (Ta-DCMS). The Ta-DCMS alloy films are only ~70% dense due to both inter- and intra-columnar porosity. In contrast, the Ta-HIPIMS layers exhibit no inter-columnar porosity and are essentially fully dense. The mechanical properties of Ta-HIPIMS films are significantly improved with hardness and elastic modulus values of 28.0 and 328 GPa compared to 15.3 and 289 GPa for reference Ta-DCMS films.

[a)] Author to whom correspondence should be addressed. Electronic mail: olof.tengstrand@liu.se

I. INTRODUCION

Transition metal (TM) nitride film growth by physical vapor deposition (PVD) techniques in the absence of ion irradiation requires elevated substrate temperatures to provide sufficient adatom mobility for obtaining dense layers. Without external heating during growth, films are underdense and exhibit poor mechanical properties.[1] Irradiation of the growing film with inert-gas ions to provide continuous near-surface ion mixing and enhanced surface adatom mobilities has been utilized to improve film density.[2,3] However, the densification often leads to trapping of gas ions and recoil implantation of surface atoms into interstitial sites, which induces large compressive stresses.[4]

We recently reported a novel PVD approach for the growth of dense, hard, and low stress refractory TM nitride thin films without external heating. TiN was used as a model materials system and we employed hybrid high-power pulsed and dc magnetron co-sputtering (HIPIMS/DCMS)[5–7] to grow $Ti_{1-x}Ta_xN$ alloys.

Here, we apply this strategy to a more complex alloy, $Ti_{1-x-y}Al_xTa_yN$, chosen based upon the importance of $Ti_{1-x}Al_xN$ films for metal cutting operations.[8–14] Moreover, it has been shown that alloying TiAlN with TaN enhances hardness, thermal stability, and oxidation resistance.[13,15–17]

Separate Ti and Al targets operated in DCMS mode maintain a high deposition rate R_s, while the HIPIMS-powered Ta target serves as a pulsed source of energetic Ta^+/Ta^{2+} metal ions. A pulsed negative substrate bias, V_s = 160 V, is applied in synchronous with the Ta-ion portion of each HIPIMS pulse in order to provide film densification by heavy Ta^+/Ta^{2+} irradiation, while minimizing the effects of Ar^+ bombardment leading to compressive stress. During DCMS deposition between HIPIMS pulses, the substrate is at floating potential, V_f = 12 V; hence, the energy of rare-gas ions incident at the growing film surface is below the lattice-atom displacement threshold.

We show that with as little as 8 mol% TaN incorporated in $Ti_{0.41}Al_{0.51}Ta_{0.08}N$ alloys, dense films with high hardness and relatively low stress σ can be obtained without using a substrate heater. Plasma heating results in a maximum film growth temperature T_s = 150 °C during the 50 min deposition of 2.6 μm-thick layers on Si(001) substrates. The film hardness H and elastic modulus E increase from 15.3 and 289 GPa for reference $Ti_{0.41}Al_{0.51}Ta_{0.08}N$ films (stress σ = +1.7 GPa) deposited purely by DCMS to 28.0 and 328 GPa for $Ti_{0.41}Al_{0.51}Ta_{0.08}N$ layers (σ = -1.6 GPa) grown by HIPIMS/DCMS co-sputtering.

II. EXPERIMENTAL PROCEDURES

$Ti_{0.41}Al_{0.51}Ta_{0.08}N$ films are grown in a CC800/9 CemeCon AG magnetron sputtering system[18], with a base pressure of 3.8×10^{-7} Torr ($5\text{x}10^{-5}$ Pa), equipped with rectangular 8.8×50 cm^2 Ti, Al, and Ta targets. The Ta target is mounted directly in front of, and parallel to, the substrate holder while the Ti and Al targets are mounted symmetrically on opposing sides of the Ta target with a 21° angle between the substrate normal and that of each target. The distance between the substrate and each target is 18 cm. The substrates are 2×1 cm^2 Si(001) wafers which are cleaned and degreased in successive ultrasonic baths of acetone and isopropyl alcohol, and blown dry in dry N_2. They are then mounted in the growth chamber with clips such that their long sides are parallel to the long sides of the targets.

The Ta target is operated in HIPIMS mode, while the Al and Ti targets are operated in DCMS mode (Ta-HIPIMS/Ti-DCMS/Al-DCMS, or simply Ta-HIPIMS). Reference TiAlTaN alloys are grown in pure DCMS mode (Ta-DCMS).

Prior to film growth, the system is degassed using two resistive heaters, each operated at 2 kW for 1 h, resulting in a temperature T_s = 150 °C at the substrate position. The power is then switched off and T_s is allowed to decrease to $\lesssim$ 120 °C before initiating film growth. No external substrate

heating is applied during deposition and T_s, monitored with a calibrated thermocouple bonded to a dummy substrate, reaches a maximum ~150 °C due to plasma heating.

During all film-growth experiments, the Ar flow rate is set to 350 cm^3/min (sccm) with an N_2/Ar ratio of 0.2. The N_2 flow is regulated by a feedback loop to maintain the total gas pressure constant at 3 mTorr (0.4 Pa).

The TaN concentration in $Ti_{1-x-y}Al_xTa_yN$ films is controlled by the average power to the HIPIMS target. Here, the HIPIMS average target power is set to 1.5 kW with a pulse energy E_p = 15 J and a frequency of 100 Hz (2% duty cycle), corresponding to a peak target current density J_T = 0.93 A/cm^2 during each pulse. The dc power to the Ti and Al targets is set to 6.0 and 4.3 kW.

$Ti_{1-x-y}Al_xTa_yN$ film compositions x and y are determined by energy-dispersive x-ray spectroscopy (EDS) in a LEO 1550 scanning electron microscopy (SEM) instrument equipped with an AZtec X-max EDS system, operated at 20 kV. N/(Ti+Al+Ta) fractions and background impurity concentrations are determined by time-of-flight elastic recoil detection analysis (TOF-ERDA) which is sensitive to light elements. In the latter measurements, a 36 MeV $^{127}I^{8+}$ beam is incident at 67.5° relative to the sample surface normal with the detector at a 45° recoil scattering angle.[19] ERDA data are analyzed using the CONTES code.[20]

In the Ta-DCMS configuration, power to the Ti and Al targets is maintained at 6.0 and 4.3 kW, while the dc power to the Ta target, 0.45 kW, is set, based upon calibration curves, to obtain alloy films with the same composition as in the Ta-HIPIMS configuration. The use of a lower dc power in this case (compared to Ta-HIPIMS) is due to the fact that ionization of sputtered metal flux is negligible during Ta-DCMS;[21] hence, there is no significant loss in deposition rate due to ionized sputter-ejected species attracted back to the target as observed during HIPIMS.[22,23] The Ta-DCMS films are grown at floating potential (V_s = V_f = 12 V). Film thicknesses, 2.6 μm, are determined

from film fracture cross-sectional SEM images obtained in a LEO 1550 instrument operated at 5 kV. Deposition rates are ~50 nm/min for both Ta-DCMS and Ta-HIPIMS deposition.

For growth of Ta-HIPIMS films, a substrate bias voltage, $V_s = 160$ V, is applied in synchronous with the 200 μs metal-ion-rich portion of each HIPIMS pulse, as determined by time-resolved ion mass spectroscopy analyses at the substrate position.[5] The metal-rich pulse begins at $t_{offset} = 50$ μs following pulse initiation (t = 0 μs) with Ta^+ and Ta^{2+} metal-ion fluxes incident at the film growth surface. At all other times, the Si(001) substrates are at a floating potential. The average energies of incident Ta^+ and Ta^{2+} ions are 9.0 and 9.3 eV, with maximum flux intensities of 3.1×10^6 and 4.3×10^6 cps. The doubly-ionized Ta^{2+} fraction $Ta^{2+}/(Ta^++Ta^{2+})$ of the metal-ion flux during HIPIMS pulses is 0.54. A more detailed description of the resulting Ta^+/Ta^{2+} irradiation conditions is described in Ref 5.

In order to directly compare the change in nanostructure upon switching between the two different sputtering modes, we deposit, in addition to single layers, Ta-DCMS/Ta-HIPIMS/Ta-DCMS trilayer stacks with total thicknesses of ~ 2.2 μm and analyze them by cross-sectional transmission electron microscopy (XTEM) using an analytical FEI Tecnai G2 TF 20 UT transmission electron microscope operated at 200 kV. The Ta-DCMS under- and overlayers, as well as the intermediate Ta-HIPIMS layers, are grown under the same conditions as for the corresponding single layers.

XTEM samples are prepared by mechanical grinding and polishing, followed by Ar^+ ion milling, with sample rotation, using a Precision Ion Milling System (PIPS) operating at 5 kV with an incidence angle of 6°. Final thinning is carried out at lower ion energy and lower incidence angle (< 1 keV and 5°, respectively) for 60 min.

ω-2θ x-ray diffraction (XRD), x-ray reflectivity (XRR), and $\sin^2\Psi$ measurements for residual stress determination are performed in a Philips X'Pert MRD system operated with point-focus Cu K_α radiation. The XRD measurements are symmetric ω-2θ scans with a 2θ range from 30 to 50° in steps of 0.1° and a collection time of 10 s/step. Relaxed lattice parameters are determined from measurements acquired at the strain-free tilt angle $\Psi^* = \arcsin\left[\{2\nu/(1+\nu)\}^{1/2}\right]$,[24] in which ν is Poisson's ratio. The $\sin^2\Psi$ method is based upon Hooke's law of linear elasticity,

$$\varepsilon(\Psi) = \frac{1+\nu}{\mathrm{E}}\sigma\sin^2\Psi - \frac{2\nu}{\mathrm{E}}\sigma. \quad (1)$$

$\varepsilon(\Psi)$ in Eq. 1 is the film strain obtained from

$$\varepsilon(\Psi) = \frac{d_\Psi - d_o}{d_o}, \quad (2)$$

for which the lattice spacings d_Ψ are determined from the positions of the cubic 002 Bragg reflections at ten different Ψ tilt angles ranging from 0 to 71.57°, with Ψ steps that produce equally spaced data points along the $\sin^2\Psi$ axis. Because of the presence of a tilted fiber texture, which is pronounced for Ta-DCMS films, we performed measurement for both positive and negative Ψ angles as recommended in ref. 24. The relaxed lattice spacing d_o is calculated from the relaxed lattice parameter a_o, obtained at the strain-free tilt angle Ψ^*. Elastic moduli E in Eq. 1 are acquired from nanoindentation measurements with a Poisson's ratio ν = 0.25, calculated by Sangiovanni et al.[25] for $Ti_{0.47}Al_{0.47}Ta_{0.06}N$.

Nanoindentation measurements are carried out in an IBIS Nanoindenter equipped with a sharp Berkovich diamond probe calibrated using a fused silica standard and a $Ti_{0.50}Al_{0.50}N$ reference sample. A minimum of 25 indents is made in each specimen with maximum loads of 15 mN. Indentation depths range from 170 nm to 220 nm, but are never allowed to exceed 10% of the film

thickness in order to minimize substrate effects. Film hardnesses H and elastic moduli E are obtained using the method described by Oliver and Pharr.[26]

III. RESULTS

A. TiAlTaN film compositions

The compositions of both Ta-HIPIMS and Ta-DCMS films, as determined by EDS and TOF-ERDA, are $Ti_{0.41}Al_{0.51}Ta_{0.08}N$. All films are stoichiometric with N/(Ti+Al+Ta) = 1.00±0.05 and the uncertainty in the reported metal concentrations on the cation sublattice is less than ±1 %. Oxygen and carbon concentrations are 1.6-2.0 and ≤ 0.2 at%, respectively, in Ta-DCMS films. For the Ta-HIPIMS films, oxygen concentrations are ≤ 0.4 at% while carbon is below detection limits. Trapped Ar concentrations in both sets of films are < 0.5 at%.

B. TiAlTaN nanostructures

Fig. 1 shows typical ω-2θ scans acquired from $Ti_{0.41}Al_{0.51}Ta_{0.08}N$ films as a function of the positive tilt angle Ψ from 0° to 71.6°, with Ψ -values chosen such that $\sin^2\Psi$ ranges from 0 to 0.9 in steps of 0.1, for (a) Ta-DCMS films grown with V_s = 12 V, and (b) Ta-HIPIMS films grown with a metal-ion-synchronized substrate bias V_s = 160 V. The positions of NaCl-structure TaN[27], TiN[28], AlN[29], and wurtzite w-AlN[30] peaks are indicated in the figure.

The x-ray diffraction patterns in Fig. 1 indicate that all films are single-phase NaCl-structure solid solutions. Typical 111 and 002 diffraction peak intensities for Ta-DCMS films, Fig. 1(a), when compared to corresponding intensities from TiN[28] and $Ti_{0.5}Al_{0.5}N$[31] powder diffraction patterns, reveal a 002 preferred orientation. The strain-free Ta-DCMS 002 peak position, obtained at the strain-free tilt angle Ψ^*, is 43.0°, yielding a relaxed lattice parameter a_o = 4.20±0.05 Å. The peaks shift to lower diffraction angles with increasing tilt angle Ψ, revealing that the films are in

tension with a stress value of +1.7 ± 0.4 GPa, consistent with an underdense nanostructure.[32] All peaks are higher in intensity and at larger diffraction angles compared to the corresponding reflections from Ta-HIPIMS films (Fig. 1(b)).

Comparing the relative 111 and 002 peak intensities to those from TiN[28] and $Ti_{0.5}Al_{0.5}N$[31] in the powder diffraction database shows that Ta-HIPIMS films have a 111 preferred orientation. The low-intensity, broad 111 and 002 diffraction peaks indicate that the Ta-HIPIMS layers have a smaller average grain size than Ta-DCMS layers and/or exhibit inhomogeneous strain. The strain-free Ta-HIPIMS 002 peak position is 42.6° corresponding to a relaxed lattice parameter a_o = 4.24±0.02 Å. The peak shift as a function of the tilt angle Ψ reveals a residual compressive stress of -1.6 ± 0.2 GPa.

Fig. 2 consists of cross-sectional SEM (XSEM) images of (a) Ta-DCMS and (b) Ta-HIPIMS films. The Ta-DCMS layer has an extremely open columnar structure with individual columns appearing as free-standing pillars. The column tops are facetted, giving rise to atomic shadowing during deposition and, thus, a very rough surface. The overall structure corresponds to zone 1 in the Thornton structure-zone diagram,[1,33] which is characterized by low adatom mobility and essentially no bulk diffusivity. The Ta-HIPIMS film in Fig. 2(b) exhibits a dense, columnar, zone-T structure with rounded column tops and a much smoother surface.

Film densities ρ are determined based upon the critical angle of total reflection θ_C obtained from low angle x-ray reflectivity (XRR) measurements[24]. Thus, Ta-DCMS films have measured densities which are ~70% of the maximum theoretical values, while Ta-HIPIMS layers are essentially fully dense. The large difference is consistent with the XSEM results shown in Fig. 2.

1. ***Ta-DCMS/Ta-HIPIMS/Ta-DCMS trilayer***

Fig. 3 is a set of bright-field XTEM images, with selected-area electron diffraction (SAED) patterns, obtained from a trilayer Ta-DCMS/Ta-HIPIMS/Ta-DCMS sample grown on Si(001). The interfaces between the individual layers are indicated by dashed lines. Since the composition of all three layers is the same, $Ti_{0.41}Al_{0.51}Ta_{0.08}N$, the image contrast is primarily due to differences in layer-density and nanostructure.

The bottom Ta-DCMS layer in Fig. 3 has a columnar nanostructure, with an average column width $\langle d \rangle = 30\pm10$ nm near the top, and pronounced intercolumnar voids. The columns exhibit uniform contrast with some dark bands which arise from sample-bend contours. Individual nanocolumns are single crystals which grow via local epitaxy. The SAED pattern acquired from the lower Ta-DCMS layer in Fig. 3(f) exhibits only NaCl reflections, consistent with XRD results in Fig. 1. The interface between the lower Ta-DCMS layer and the middle Ta-HIPIMS layer is sharp, indicating that heavy-metal irradiation results in an immediate change in intracolumnar nanostructure, even though columns continue via local epitaxy throughout the entire trilayer film, as is evident by the uniform phase contrast. The Ta-HIPIMS layer exhibits a speckle contrast due to local strain-fields generated by ion-induced irradiation[34], which explains the corresponding broadening of the diffraction peak in Fig. 1(b).

The SAED pattern obtained from the Ta-HIPIMS layer, Fig. 3(e), consists of diffraction rings corresponding to the NaCl structure. There is, however, an additional, weak hexagonal w-AlN(100) ring marked with an arrow.

The interface between the middle Ta-HIPIMS and upper Ta-DCMS layer, as metal-ion irradiation is switched off, is also abrupt with the upper layer exhibiting an open columnar structure, similar to that of the initial Ta-DCMS layer. The columns in the upper layer increase in

diameter, and the voids become more open as the layer thickness increases. The faceted tops develop due to kinetic roughening of columns growing by local epitaxy.[1] SAED patterns acquired from the lower and upper Ta-DCMS layers are very similar, neither contains w-AlN diffraction rings.

In order to reveal additional nanostructural details of the Ta-HIPIMS layer, we acquire dark-field XTEM images of the trilayer in which the objective aperture includes segments of the 111 and 002 NaCl structure rings with diffraction vectors along the film growth direction. This illuminates coherently-diffracting grains and provides an estimate of their average shape and size. The majority of the columns shown in Fig. 4 persist through the Ta-HIPIMS layer. The Ta-HIPIMS region of the XTEM foil is clearly thicker than that of the surrounding Ta-DCMS layers. Thus, the Ta-HIPIMS layer has a lower ion-etching rate, further evidence of its higher density. Note that some of the Ta-HIPIMS columns in Fig. 4 are truncated due to the non-uniform foil thickness. The average Ta-HIPIMS column width is 48 ± 14 nm.

The total volume, and dispersed distribution, of w-AlN phase in the Ta-HIPIMS layers is too small to be observed in dark-field images. Fig. 5(a) is a lattice-resolution image of a portion of a Ta-HIPIMS column together with a fast Fourier transform (FFT) pattern of the image. Just as in the SAED, there are 100 w-AlN reflections in the FFT pattern. An inverse FFT was obtained using the reflections highlighted with white arrowheads. The resultant pattern, Fig. 5(b), reveals a w-AlN grain, which is outlined with a dashed line in the higher-magnification image Fig. 5(c). With further increase in magnification, Fig. 5(d), a lattice spacing of 2.75 Å is obtained, which is larger than the 2.45 Å 111 interplanar spacing of NaCl-structure TiAlTaN and corresponds to the 100 reflection of w-AlN. Performing such analysis in multiple areas, we conclude that the average w-

AlN grain size is 5$\pm$3 nm. Such grains are located predominantly at column boundaries in the Ta-HIPIMS layer.

C. Nanoindentation hardness and elastic moduli

The nanoindentation hardness H of Ta-HIPIMS films, 28.0±1.0 GPa, is considerably higher than that of Ta-DCMS layers (15.3±0.8 GPa). This is due primarily to the much higher film density. The Ta-HIPIMS films also have higher elastic moduli, 328 ± 14 GPa, compared to 289 ± 10 GPa for Ta-DCMS layers.

IV. DISCUSSION

Based upon XRD, SAED, and TEM results, 2.6-μm-thick Ta-DCMS $Ti_{0.41}Al_{0.51}Ta_{0.08}N$ reference films deposited at $T_s \leq 150$ °C with $V_s = 12$ V are single phase, metastable, NaCl-structure solid solutions with a relaxed lattice constant of 4.20 Å. The average Ta-DCMS column diameter is <d> = 30$\pm$10 nm. The layers are highly underdense with both inter- and intracolumnar porosity due to low adatom mobilities resulting from the very-low film growth temperature ($T_s/T_m \lesssim 0.14$). The low film density, ~70% as determined from XRR, results in the layers exhibiting tensile stress, +1.7 GPa, and having a low hardness, 15.3 GPa, and elastic modulus, 289 GPa.

Heavy-metal ion irradiation during film growth in the hybrid Ta-HIPIMS/Ti-DCMS/Al-DCMS mode, eliminates intracolumnar voids yielding essentially fully-dense Ta-HIPIMS layers and a columnar NaCl crystal structure with an average column diameter <d> = 48$\pm$14 nm. Dispersed small wurtzite-structure AlN grains (not detectable by XRD), with average size 5$\pm$3 nm, are formed at localized regions along column boundaries in the Ta-HIPIMS layers and explains the slightly larger relaxed lattice constant of the NaCl structure phase in Ta-HIPIMS films, 4.24 Å, compared to 4.20 Å for Ta-DCMS films.

Ta-HIPIMS layers, as a result of their higher density, have dramatically higher hardness and elastic modulus values, H = 28.0 GPa and E = 328 GPa, than Ta-DCMS films with the same overall composition. In addition, we obtain a significant increase in the H^3/E^2 ratio, an indication of increased wear resistance[35], from 0.04 for Ta-DCMS to 0.20 in the case of Ta-HIPIMS layers. The residual film stress remains relatively low, σ = -1.6 GPa, but switches to compressive due to the combination of ion-irradiation induced densification and residual lattice defects. Ta-HIPIMS layers also have much smoother surfaces than Ta-DCMS layers (Fig. 2).

The effective near-surface mixing caused by Ta^+/Ta^{2+} irradiation during Ta-HIPIMS growth provides densification. Monte Carlo TRIM[36] simulation results for 160 eV Ta irradiation show that Ta^+ collision cascades extend over depths of 13-19 Å for N, Ta, Al, and Ti recoils, while primary Ta^+ and Ta^{2+} ions penetrate deeper, ξ_{ion} ~25 and ~30 Å, respectively, due to their higher mass and, hence, decreased scattering angles. The shallow collision cascades continuously fill residual vacancies, which form due to the extremely-low growth temperature. In the present experiments, the TiAlN thickness h_{TiAlN} deposited between pulses is 0.09 Å (0.04 ML). Thus, the Ta^+/Ta^{2+} ion penetration range $\xi_{ion} \gg h_{TiAlN}$, leading to effective dynamic near-surface mixing during the HIPIMS pulses. Because of the large mass difference between the heavy Ta ions and the other film constituents, ion irradiation creates a high density of low-energy N, Al, and Ti recoils wich provide film densification. Enhanced atom mobilities in the near surface region also lead to the formation of nano-size w-AlN grains at column boundaries. The size and number density of these small precipitates is not sufficiently large to cause renucleation as columns exhibit continuous local epitaxy and extend throughout the Ta-HIPIMS layer.

XTEM bright- and dark-field images show speckle contrast which arises from local strain fields associated with residual radiation damage. During high-temperature annealing of single-phase

TiAlN films, it has been observed that coherent c-AlN grains evolve through spinodal decomposition which introduces a shoulder in NaCl-structure x-ray reflections.[37–39] For the low growth temperature employed in the current study, XRD shoulder peak are not observed; rather, peak broadening indicates the possible formation of AlN- and TaN-rich regions. The presence of defects, which introduces local strain in NaCl-structure columns, may also contribute to enhanced Ta-HIPIMS film hardness.

V. CONCLUSIONS

We show that dc magnetron co-sputtering (HIPIMS/DCMS) can be used to grow dense and hard $Ti_{0.41}Al_{0.51}Ta_{0.08}N$ alloys without external heating ($T_s \leq 150$ ºC). Using substrate bias synchronized with the Ta^+/Ta^{2+} portion of the HIPIMS-pulses provides effective near-surface atomic mixing resulting in film densification. The substrate potential $V_s = V_f$ at all other time, which minimizes Ar^+ bombardment that typically leads to high compressive stress. DCMS sputtering from the Ti and Al targets maintains the deposition rate equal to that of Ta-DCMS layers. The resulting films are columnar with no observable intercolumnar porosity and essentially fully dense. The hardness and elastic moduli of Ta-HIPIMS layers are 28.0 and 328 GPa.

In sharp contrast, reference $Ti_{0.41}Al_{0.51}Ta_{0.08}N$ layers grown under the same conditions except that all targets are operated in DCMS mode, are only ~70% dense and exhibit both inter- and intracolumnar porosity which degrade the mechanical properties compared to the Ta-HIPIMS layers. The hardness and elastic modulus of the Ta-DCMS reference films are 15.3 and 289 GPa.

ACKNOWLEDGMENTS

Financial support from the Swedish Research Council VR Grants 2013-4018 and 2014-5790, VINN Excellence Center *Functional Nanoscale Materials* (FunMat), the Åforsk foundation grant #16-359, the Swedish Government Strategic Research Area in Materials Science on Functional

Materials at Linköping University (SFO-Mat-LiU 2009-00971), and the Knut and Alice Wallenberg Foundation Scholar Grant 2011.0143 are gratefully acknowledged. The authors would like to acknowledge Uppsala University for giving us access to the Tandem Laboratory for TOF-E- ERDA equipment. We also thank Dr. Jens Jensen (Department of Physics, Chemistry, and Biology (IFM), Linköping University) for carrying out the TOF-ERDA measurements and for valuable discussions of the results.

REFERENCES

[1] I. Petrov, P.B. Barna, L. Hultman, and J.E. Greene, J. Vac. Sci. Technol., A, **21**, S117 (2003).

[2] D. Gall, I. Petrov, N. Hellgren, L. Hultman, J.E. Sundgren, and J.E. Greene, J. Appl. Phys. **84**, 6034 (1998).

[3] G. Håkansson, J.-E. Sundgren, D. McIntyre, J.E. Greene, and W.-D. Münz, Thin Solid Films **153**, 55 (1987).

[4] I. Petrov, L. Hultman, J.-E. Sundgren, and J.E. Greene, J. Vac. Sci. Technol., A, **10**, 265 (1992).

[5] G. Greczynski, J. Lu, S. Bolz, W. Kölker, C. Schiffers, O. Lemmer, I. Petrov, J.E. Greene, and L. Hultman, J. Vac. Sci. Technol., A, **32**, 41515 (2014).

[6] G. Greczynski, J. Lu, M.P. Johansson, J. Jensen, I. Petrov, J.E. Greene, and L. Hultman, Surf. Coat. Technol. **206**, 4202 (2012).

[7] G. Greczynski, J. Lu, M. Johansson, J. Jensen, I. Petrov, J.E. Greene, and L. Hultman, Vacuum **86**, 1036 (2012).

[8] M.P. Johansson Jõesaar, N. Norrby, J. Ullbrand, R. M'Saoubi, and M. Odén, Surf. Coat. Technol. **235**, 181 (2013).

[9] N. Norrby, M.P. Johansson-Jõesaar, and M. Odén, Surf. Coat. Technol. **257**, 102 (2014).

[10] A. Inspektor and P.A. Salvador, Surf. Coat. Technol. **257**, 138 (2014).

[11] S. PalDey and S.. Deevi, Mater. Sci. Eng. A **342**, 58 (2003).

[12] G. Erkens, R. Cremer, T. Hamoudi, K.-D. Bouzakis, I. Mirisidis, S. Hadjiyiannis, G. Skordaris, A. Asimakopoulos, S. Kombogiannis, J. Anastopoulos, and K. Efstathiou, Surf. Coat. Technol. **177–178**, 727 (2004).

[13] M. Kathrein, C. Michotte, M. Penoy, P. Polcik, and C. Mitterer, Surf. Coat. Technol. **200**, 1867 (2005).

[14] K.-D. Bouzakis, N. Michailidis, G. Skordaris, E. Bouzakis, D. Biermann, and R. M'Saoubi, CIRP Ann. - Manuf. Technol. **61**, 703 (2012).

[15] R. Hollerweger, H. Riedl, J. Paulitsch, M. Arndt, R. Rachbauer, P. Polcik, S. Primig, and P.H. Mayrhofer, Surf. Coat. Technol. **257**, 78 (2014).

[16] X. Sui, G. Li, C. Jiang, H. Yu, K. Wang, and Q. Wang, Int. J. Refract. Met. Hard Mater. **58**, 152 (2016).

[17] M. Pfeiler, C. Scheu, H. Hutter, J. Schnöller, C. Michotte, C. Mitterer, and M. Kathrein, J. Vac. Sci. Technol., A, **27**, 554 (2009).

[18]"CemeCon, CC800/9 HIPIMS system." [Online]. Available: http://www.cemecon.de/coating_technology/coating_units/hipims_sputter_coating_system/index_eng.html. [Accessed: 23-Aug-2016]

[19] J. Jensen, D. Martin, A. Surpi, and T. Kubart, Nucl. Instrum. Methods Phys. Res., Sect. B **268**, 1893 (2010).

[20] M.S. Janson, *CONTES Conversion of Time-Energy Spectra - a Program for ERDA Data Analysis* (2004).

[21] I. Petrov, A. Myers, J. Greene, J. Abelson, J. Vac. Sci. Technol., A, **12**, 2846 (1994).

[22] D.J. Christie, J. Vac. Sci. Technol., A, **23**, 330 (2005).

[23] M. Samuelsson, D. Lundin, J. Jensen, M.A. Raadu, J.T. Gudmundsson, and U. Helmersson, Surf. Coat. Technol. **205**, 591 (2010).

[24] M. Birkholz, *Thin Film Analysis by X-Ray Scattering* (Wiley-VCH Verlag GmbH & Co., Weinheim, 2006).

[25] D.G. Sangiovanni, V. Chirita, and L. Hultman, Thin Solid Films **520**, 4080 (2012).

[26] W.C. Oliver and G.M. Pharr, J. Mater. Res. **7**, 1564 (1992).

[27] JCPDS, TaN Powder Diffraction File: 00-049-1283.

[28] JCPDS, TiN Powder Diffraction File: 00-038-1420.

[29] JCPDS, AlN Powder Diffraction File: 00-046-1200.

[30] JCPDS, AlN Powder Diffraction File: 00-025-1133.

[31] JCPDS, (AlTi)N2 Powder Diffraction File: 01-071-5864.

[32] E. Chason, Thin Solid Films **526**, 1 (2012).

[33] J.A. Thornton, J. Vac. Sci. Technol., A, **4**, 3059 (1986).

[34] I. Petrov, L. Hultman, U. Helmersson, J.-E. Sundgren, and J.E. Greene, Thin Solid Films **169**, 299 (1989).

[35] A. Leyland and A. Matthews, Wear **246**, 1 (2000).

[36] "SRIM, Interactions of ions with matter." [Online]. Available: http://www.srim.org. [Accessed: 23-Aug-2016]

[37] N. Norrby, L. Rogström, M.P. Johansson-Jõesaar, N. Schell, and M. Odén, Acta Materialia **73**, 205 (2014).

[38] R. Rachbauer, S. Massl, E. Stergar, D. Holec, D. Kiener, J. Keckes, J. Patscheider, M. Stiefel, H. Leitner, and P.H. Mayrhofer, J. Appl. Phys. **110**, 23515 (2011).

[39] P.H. Mayrhofer, A. Hörling, L. Karlsson, J. Sjölén, T. Larsson, C. Mitterer, and L. Hultman, Appl. Phys. Lett. **83**, 2049 (2003).

FIGURES

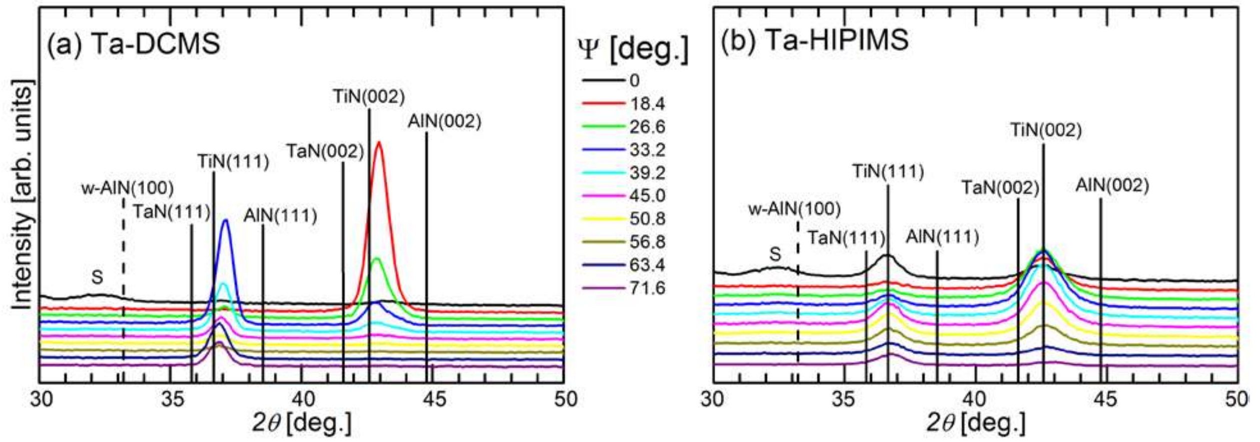

FIG. 1. (Color online) ω-2θ scans at different positive tilt angles Ψ for (a) Ta-DCMS and (b) Ta-HIPIMS films. The vertical lines in each panel correspond to the positions of c-TaN,[27] c-TiN,[28] c-AlN,[29] and w-AlN,[30] diffraction peaks from reference powder diffraction data. S indicates the position of the "forbidden" 002 reflection from the Si(001) substrate.

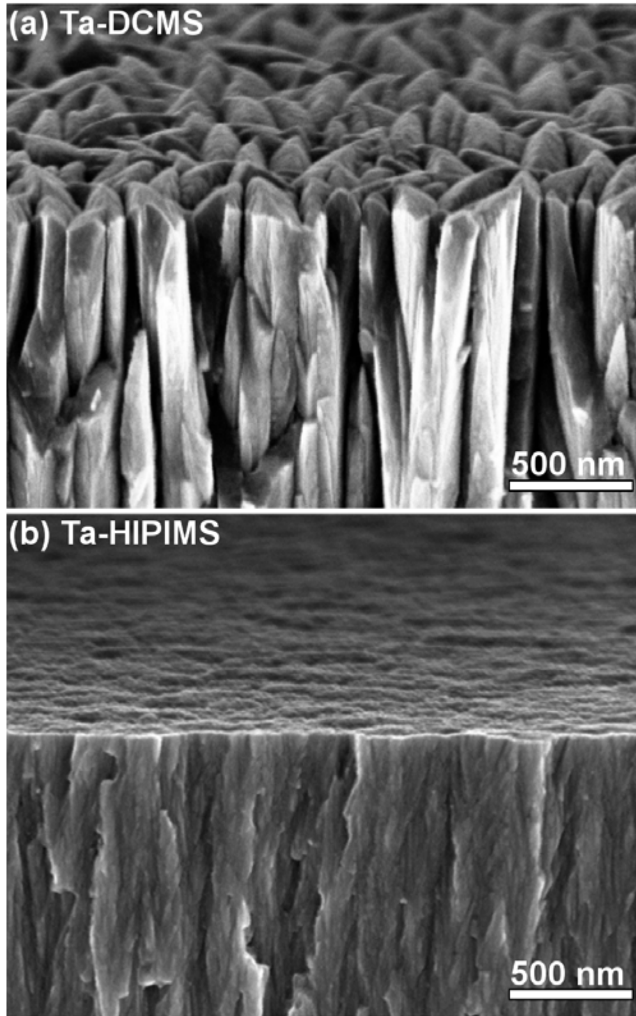

FIG. 2. Cross-sectional SEM images of (a) Ta-DCMS and (b) Ta-HIPIMS $Ti_{0.41}Al_{0.51}Ta_{0.08}N$ films.

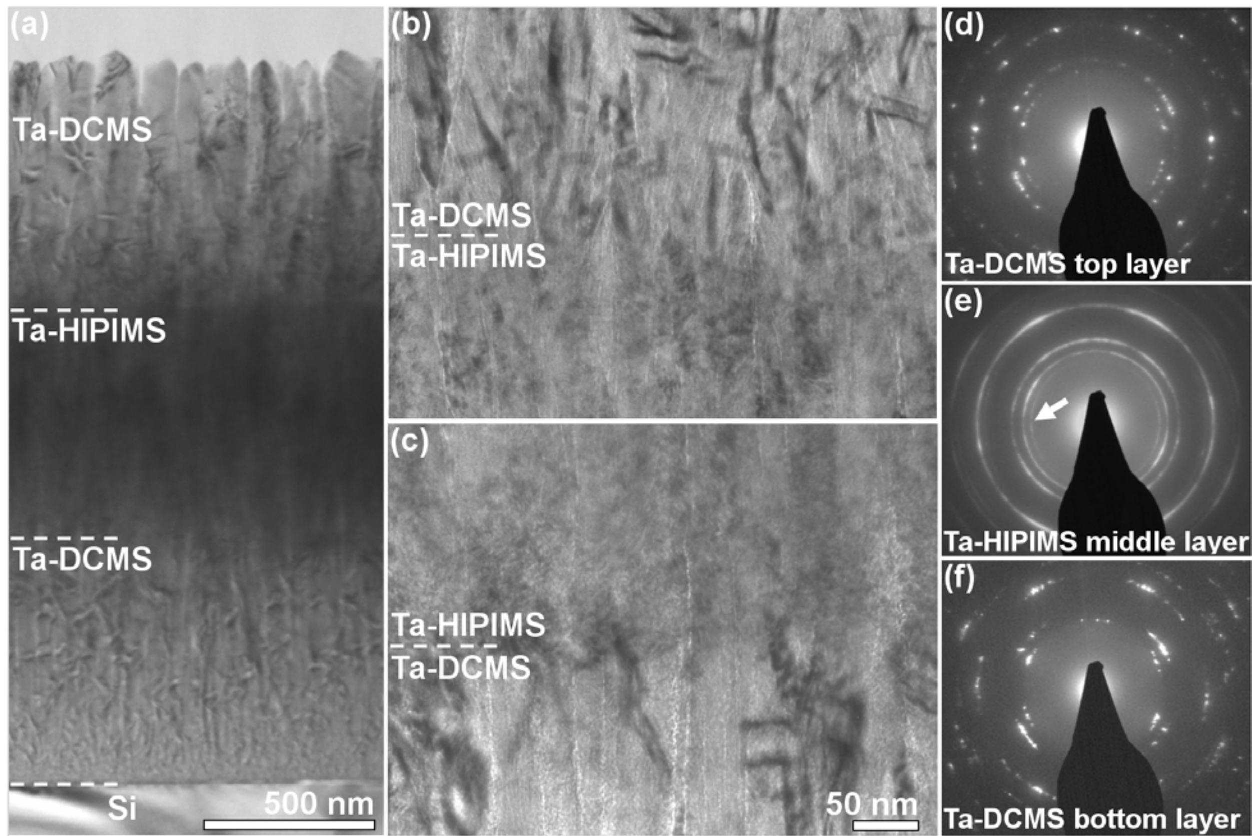

FIG. 3. (a) BF-XTEM overview image of a Ta-DCMS/Ta-HIPIMS/Ta-DCMS trilayer film. Higher resolution images of the interfaces are shown in (b) for the top/middle layers and (c) for the middle/bottom layers. SAED patterns from each individual layer are presented in (d)-(f). The arrow in (e) points to a weak diffraction w-AlN(100) ring.

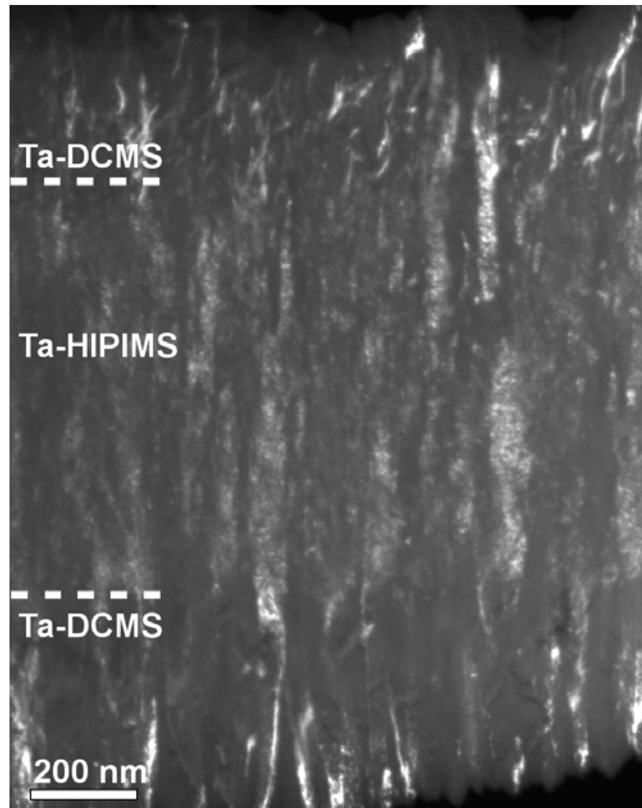

FIG. 4. Dark-field XTEM image of the trilayer sample, obtained using portions of the 111 and 002 NaCl-structure rings with diffraction vectors along the film growth direction.

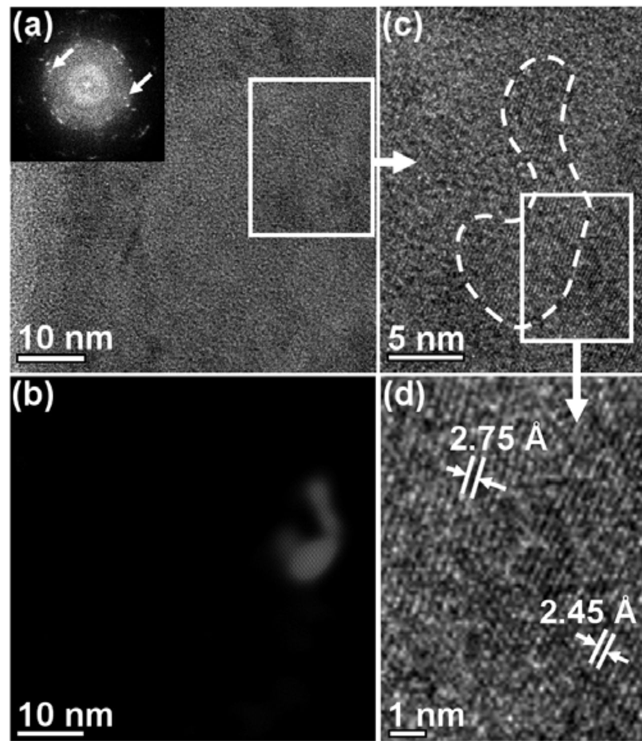

FIG. 5 (a) High resolution XTEM image of a Ta-HIPIMS $Ti_{0.41}Al_{0.51}Ta_{0.08}N$ layer. A Fourier transform in which the arrows point to w-AlN (100) reflections is shown in the inset. (b) Inverse Fourier transform obtained using only the w-AlN reflections shown in (a). (c) Higher magnification view of the region in (a) highlighted by the white rectangle. The dashed line outlines a w-AlN grain. (d) An even higher magnification view of the region in (c) outlined by the white rectangle showing the interplanar spacing of w-AlN 100 (2.75 Å) and NaCl-structure TiAlTaN 111 (2.45 Å).